MULTISCALE MODEL. SIMUL.
Vol. 12, No. 2, pp. 907–926

A PATHWAY-BASED MEAN-FIELD MODEL FOR *E. COLI* CHEMOTAXIS: MATHEMATICAL DERIVATION AND ITS HYPERBOLIC AND PARABOLIC LIMITS*

GUANGWEI SI†, MIN TANG‡, AND XU YANG§

Abstract. A pathway-based mean-field theory (PBMFT) that incorporated the most recent quantitatively measured signaling pathway was recently proposed for the *E. coli* chemotaxis in [G. Si, T. Wu, Q. Quyang, and Y. Tu, *Phys. Rev. Lett.*, 109 (2012), 048101]. In this paper, we formally derive a new kinetic system of PBMFT under the assumption that the methylation level is locally concentrated, whose turning operator takes into account the dynamical intracellular pathway and hence is more physically relevant. We recover the PBMFT proposed by Si et al. as the hyperbolic limit and connect to the Keller–Segel equation as the parabolic limit of this new model. We also present the numerical evidence to show the quantitative agreement of the kinetic system with the individual based *E. coli* chemotaxis simulator.

Key words. pathway-based mean-field model, *E. coli* chemotaxis, hyperbolic limit, parabolic limit, Keller–Segel model

AMS subject classifications. 35Q92, 92B05

DOI. 10.1137/130944199

1. Introduction.

The locomotion of *Escherichia coli* (*E. coli*) presents a tumble-and-run pattern [5], which can be viewed as a biased random walk process. In the presence of a chemoeffector with a nonzero gradient, the suppression of direction change (tumble) leads to chemotaxis toward the high concentration of chemoattractant [1, 4]. Much effort has been made to understand the chemotactic sensory system of *E. coli* (e.g., [11, 18, 32, 34]). The chemotactic signaling pathway belongs to the class of two-component sensory systems, which consists of sensors and response regulators. The chemotactic sensor complex is composed of transmembrane chemoreceptors, the adaptor protein CheW, and the histidine kinase CheA. The response regulator CheY controls the tumbling frequency of the flagellar motor [19]. Adaptation is carried out by the two enzymes, CheR and CheB, which control the kinase activity by modulating the methylation level of receptors [34]. Because of the slow adaptation process, the receptor methylation level serves as the memory of cells in a way that the cells effectively run or tumble by comparing the receptor methylation level to local environments.

In the modeling literature, bacterial chemotaxis has been described by the Keller–Segel (KS) model at the population level [23], where the drift velocity is given by the empirical functions of the chemoeffector gradient. It has successfully explained

*Received by the editors November 5, 2013; accepted for publication (in revised form) April 14, 2014; published electronically June 26, 2014.
http://www.siam.org/journals/mms/12-2/94419.html

†Center for Quantitative Biology, Peking University, Beijing, China, 100871 (gwsi@pku.edu.cn). This author was partially supported by NSF of China under grants 11074009 and 10721463 and the MOST of China under grants 2009CB918500 and 2012AA02A702.

‡Corresponding author. Institute of Natural Sciences, Department of Mathematics and MOE-LSC, Shanghai Jiao Tong University, 200240, Shanghai, China (tangmin@sjtu.edu.cn). This author is partially supported by Natural Science Foundation of Shanghai under grant 12ZR1445400, NSFC 11301336, and Shanghai Pujiang Program 13PJ140700.

§Department of Mathematics, University of California, Santa Barbara, CA 93106 (xuyang@math.ucsb.edu). This author was partially supported by the Regents Junior Faculty Fellowship of University of California, Santa Barbara.

chemotactic phenomena in slowly changing environments [31]; however, it has failed to predict them in rapidly changing environments [36], including the so-called volcano effects [10, 28]. Additionally, the KS model has also been mathematically proved to present nonphysical blowups in high dimensions when initial mass goes beyond the critical level [6, 7, 8]. In order to understand bacterial behavior at the individual level, kinetic models have been developed by considering the velocity-jump process [3, 21, 30], and the KS model can be derived by taking the hydrodynamic limit of kinetic models (e.g., [12, 17]). All the above-mentioned models are phenomenological and do not take into account the internal signal transduction and adaptation process. It is especially hard to justify the physically relevant turning operator in the kinetic model.

Today, modern experimental technologies have been able to quantitatively measure the dynamics of signaling pathways of *E. coli* [2, 13, 26, 29], which has led to the successful modeling of the internal pathway dynamics [24, 25, 33]. These works made possible the development of predictive agent-based models that include the intracellular signaling pathway dynamics. It is of great biological interest to understand the molecular origins of chemotactic behavior of *E. coli* by deriving a population-level model based on the underlying signaling pathway dynamics. In the pioneering work of [15, 16, 35], the authors derived macroscopic models by studying the kinetic chemotaxis models incorporating linear models for signaling pathways. In [27], the authors developed a pathway-based mean field theory (PBMFT) that incorporated the most recent quantitatively measured signaling pathway and explained a counterintuitive experimental observation which showed that in a spatial-temporal fast-varying environment, there exists a phase shift between the dynamics of ligand concentration and the center of mass of the cells [36]. In particular, when the oscillating frequency of ligand concentration is comparable to the adaptation rate of *E. coli*, the phase shift becomes significant. Apparently this is a phenomenon that cannot be explained by the KS model.

In this paper, we study the PBMFT for *E. coli* chemotaxis based on kinetic theory. Specifically we derive a new kinetic system whose turning operator takes into account the dynamic intracellular pathway. What is different about this new system is that, compared with those kinetic models in [3, 21, 30], neither the turning operator nor the methylation level depends on the chemical gradient explicitly, which is more consistent with the recent computational studies in [27]. Additionally, all parameters can be measured by experiment, and quantitative matching with experiments can be done. The key observation here is that the methylation level is locally concentrated in the experimental environment. We formally obtain the KS limit in the parabolic scaling and the PBMFT proposed in [27] in the hyperbolic scaling of the kinetic system by taking into account the disparity between the time scales of tumbling, adaptation, and experimental observation. The assumption on the methylation difference and the quasi-static approximation on the density flux in [27] can be understood explicitly in this new system. We also verify the agreement of the kinetic system with the signaling pathway-based *E. coli* chemotaxis agent-based simulator (SPECS [22]) by the numerical simulation in the environment of spatial-temporal varying ligand concentration.

The rest of the paper is organized as follows. We introduce the pathway-based kinetic model incorporating the intracellular adaptation dynamics in section 2. In section 3, assuming the methylation level is locally concentrated, we are able to derive the kinetic system independent of the methylation level in one dimension. Furthermore, the modeling assumption will be justified both analytically and numerically. By

Hilbert expansion, section 4.2 provides the recovery of the PBMFT model proposed in [27] in the hyperbolic scaling of the new system, illustrates why the KS model is valid in the slow varying environments, and shows the numerical evidence of the quantitative agreement of the system with SPECS. The two-dimensional moment system is derived in section 5, and we make conclusive remarks in section 6.

2. Description of the kinetic model. We shall start from the same kinetic model used in [27], which incorporates the most recent progress on modeling of the chemosensory system [26, 33]. The model is a one-dimensional two-flux model given by

$$\frac{\partial P^+}{\partial t} = -\frac{\partial (v_0 P^+)}{\partial x} - \frac{\partial (f(a)P^+)}{\partial m} - \frac{z(a)}{2}(P^+ - P^-), \tag{2.1}$$

$$\frac{\partial P^-}{\partial t} = \frac{\partial (v_0 P^-)}{\partial x} - \frac{\partial (f(a)P^-)}{\partial m} + \frac{z(a)}{2}(P^+ - P^-). \tag{2.2}$$

In this model, each single cell of *E. coli* moves in either the "+" or the "−" direction with a constant velocity v_0. $P^{\pm}(t, x, m)$ is the probability density function for the cells moving in the "±" direction, at time t, position x, and methylation level m. The global existence results for the linear internal dynamic case has been established in [14] in one dimension as well as in [9] for higher dimensions.

The intracellular adaptation dynamics is described by

$$\frac{\mathrm{d}m}{\mathrm{d}t} = f(a) = k_R(1 - a/a_0), \tag{2.3}$$

where the receptor activity $a(m, [L])$ depends on the intracellular methylation level m as well as the extracellular chemoattractant concentration $[L]$, which is given by

$$a = \big(1 + \exp(NE)\big)^{-1}. \tag{2.4}$$

According to the two-state model in [24, 25], the free energy is

$$E = -\alpha(m - m_0) + f_0([L]), \qquad \text{with} \quad f_0([L]) = \ln\left(\frac{1 + [L]/K_I}{1 + [L]/K_A}\right). \tag{2.5}$$

In (2.3), k_R is the methylation rate, and a_0 is the receptor preferred activity that satisfies $f(a_0) = 0$, $f'(a_0) < 0$. N, m_0, K_I, K_A represent the number of tightly coupled receptors, basic methylation level, and dissociation constant for inactive receptors and active receptors, respectively.

We take the tumbling rate function $z(m, [L])$ in [27],

$$z = z_0 + \tau^{-1}(a/a_0)^H, \tag{2.6}$$

where z_0, H, τ represent the rotational diffusion, the Hill coefficient of flagellar motor's response curve, and the average run time, respectively. We refer the readers to [27] and the references therein for the detailed physical meanings of these parameters.

More generally, the kinetic model incorporating the chemosensory system is given as

$$\partial_t P = -\boldsymbol{v} \cdot \nabla_{\boldsymbol{x}} P - \partial_m (f(a)P) + Q(P, z), \tag{2.7}$$

where $P(t, \boldsymbol{x}, \boldsymbol{v}, m)$ is the probability density function of bacteria at time t, position $\boldsymbol{x}$, moving at velocity $\boldsymbol{v}$, and methylation level m.

The tumbling term $Q(P,z)$ is

(2.8)
$$Q(P,z) = \fint_\Omega z(m,[L],\boldsymbol{v},\boldsymbol{v}')P(t,\boldsymbol{x},\boldsymbol{v}',m)\,\mathrm{d}\boldsymbol{v}' - \fint_\Omega z(m,[L],\boldsymbol{v}',\boldsymbol{v})\,\mathrm{d}\boldsymbol{v}'P(t,\boldsymbol{x},\boldsymbol{v},m),$$

where Ω represents the velocity space and the integral

$$\fint = \frac{1}{|\Omega|}\int_\Omega, \qquad \text{where } |\Omega| = \int_\Omega \mathrm{d}\boldsymbol{v},$$

denotes the average over Ω. $z(m,[L],\boldsymbol{v},\boldsymbol{v}')$ is the tumbling frequency from $\boldsymbol{v}'$ to $\boldsymbol{v}$, which is also related to the activity a as in (2.6). The first term on right-hand side of (2.8) is a gain term, and the second is a loss term.

3. One-dimensional mean-field model. In this section, we derive the new kinetic system from (2.1)–(2.2) based on the the assumption that the methylation level is locally concentrated. This assumption will be justified by the numerical simulations using SPECS and the formal analysis in the limit of $k_R \to \infty$. To simplify notation, we denote $\int_0^{+\infty}$ by $\int$ in the rest of this paper.

3.1. Derivation of the kinetic system. First, we define the macroscopic quantities, forward density, backward density, forward momentum (on m), and backward momentum as follows:

$$\rho^+(x,t) = \int P^+\,\mathrm{d}m, \quad \rho^-(x,t) = \int P^-\,\mathrm{d}m, \tag{3.1}$$

$$q^+(x,t) = \int mP^+\,\mathrm{d}m, \quad q^-(x,t) = \int mP^-\,\mathrm{d}m. \tag{3.2}$$

The average methylation levels of the forward and backward cells $M^+(t,x)$, $M^-(t,x)$ are defined as

$$M^+ = \frac{q^+}{\rho^+}, \qquad M^- = \frac{q^-}{\rho^-}. \tag{3.3}$$

For simplicity, we also introduce the following notation:

$$Z^\pm = z\big(M^\pm(t,x)\big), \qquad F^\pm = f\Big(a\big(M^\pm(t,x),[L]\big)\Big). \tag{3.4}$$

Assumption A. We need the following condition to close the moment system:

$$\frac{\int (m/M^\pm - 1)^2 P^\pm\,\mathrm{d}m}{\int P^\pm\,\mathrm{d}m} \ll 1, \qquad \frac{\int (m/M^\pm - 1)^2 P^\pm\,\mathrm{d}m}{\int |m/M^\pm - 1| P^\pm\,\mathrm{d}m} \ll 1.$$

Remark 1. Physically this assumption means that distribution functions $P^\pm$ are localized in m, and the variation of averaged methylation is small in both moving directions "±."

Integrating (2.1) and (2.2) with respect to m yields the equation for ρ^+ and ρ^-,

respectively, such that

$$\begin{aligned}\frac{\partial \rho^+}{\partial t} &= -v_0\frac{\partial \rho^+}{\partial x} - \frac{1}{2}\Big(\int z(a)P^+\,dm - \int z(a)P^-\,dm\Big)\\ &\approx -v_0\frac{\partial \rho^+}{\partial x} - \frac{1}{2}\Big(\int \Big(z(M^+) + \frac{\partial z}{\partial m}\Big|_{M^+}(m-M^+)\Big)P^+\,dm\\ &\qquad - \int \Big(z(M^-) + \frac{\partial z}{\partial m}\Big|_{M^-}(m-M^-)\Big)P^-\,dm\Big)\\ &= -v_0\frac{\partial \rho^+}{\partial x} - \frac{1}{2}\Big(Z^+\rho^+ - Z^-\rho^-\Big),\end{aligned}$$

$$\begin{aligned}\frac{\partial \rho^-}{\partial t} &= v_0\frac{\partial \rho^-}{\partial x} + \frac{1}{2}\Big(\int z(a)P^+\,dm - \int z(a)P^-\,dm\Big)\\ &\approx v_0\frac{\partial \rho^-}{\partial x} + \frac{1}{2}\Big(\int \Big(z(M^+) + \frac{\partial z}{\partial m}\Big|_{M^+}(m-M^+)\Big)P^+\,dm\\ &\qquad - \int \Big(z(M^-) + \frac{\partial z}{\partial m}\Big|_{M^-}(m-M^-)\Big)P^-\,dm\Big)\\ &= v_0\frac{\partial \rho^-}{\partial x} + \frac{1}{2}\Big(Z^+\rho^+ - Z^-\rho^-\Big),\end{aligned}$$

where we have used Assumption A in the second step and the notation in (3.3), (3.4) in the third step.

Similarly, multiplying (2.1) and (2.2) by m and integrating them with respect to m gives the equation for q^+ and q^-, respectively:

$$\begin{aligned}\frac{\partial q^+}{\partial t} &= -v_0\frac{\partial q^+}{\partial x} - \int m\frac{\partial (f(a)P^+)}{\partial m}\,\mathrm{d}m - \frac{1}{2}\Big(\int mz(a)P^+\,\mathrm{d}m - \int mz(a)P^-\,\mathrm{d}m\Big)\\ &\approx -v_0\frac{\partial q^+}{\partial x} + \int \Big(f(a)|_{m=M^+} + \frac{\partial f}{\partial m}\Big|_{m=M^+}(m-M^+)\Big)P^+\,\mathrm{d}m\\ &\qquad - \frac{1}{2}\Big(\int \Big(M^+Z^+ + \frac{\partial\big(mz(a)\big)}{\partial m}(M^+)(m-M^+)\Big)P^+\,\mathrm{d}m\\ &\qquad\quad - \int \Big(M^-Z^- + \frac{\partial\big(mz(a)\big)}{\partial m}(M^-)(m-M^-)\Big)P^-\,\mathrm{d}m\Big)\\ &= -v_0\frac{\partial q^+}{\partial x} + F^+\rho^+ - \frac{1}{2}\Big(M^+Z^+\rho^+ - M^-Z^-\rho^-\Big),\end{aligned}$$

$$\begin{aligned}\frac{\partial q^-}{\partial t} &= v_0\frac{\partial q^-}{\partial x} - \int m\frac{\partial (f(a)P^-)}{\partial m}\,\mathrm{d}m + \frac{1}{2}\Big(\int mz(a)P^+\,\mathrm{d}m - \int mz(a)P^-\,\mathrm{d}m\Big)\\ &\approx v_0\frac{\partial q^-}{\partial x} + \int \Big(f(a)|_{m=M^-} + \frac{\partial f}{\partial m}\Big|_{m=M^-}(m-M^-)\Big)P^-\,\mathrm{d}m\\ &\qquad + \frac{1}{2}\Big(\int \Big(M^+Z^+ + \frac{\partial\big(mz(a)\big)}{\partial m}(M^+)(m-M^+)\Big)P^+\,\mathrm{d}m\\ &\qquad\quad - \int \Big(M^-Z^- + \frac{\partial\big(mz(a)\big)}{\partial m}(M^-)(m-M^-)\Big)P^-\,\mathrm{d}m\Big)\\ &= v_0\frac{\partial q^-}{\partial x} + F^-\rho^- + \frac{1}{2}\Big(M^+Z^+\rho^+ - M^-Z^-\rho^-\Big),\end{aligned}$$

where we have used an integration by parts and the definition of M^+ and M^- in (3.3) in the second step.

Altogether, we obtain a system for ρ^+, ρ^-, q^+, and q^-:

$$\frac{\partial \rho^+}{\partial t} = -v_0 \frac{\partial \rho^+}{\partial x} - \frac{1}{2}\Big(Z^+\rho^+ - Z^-\rho^-\Big), \tag{3.5}$$

$$\frac{\partial \rho^-}{\partial t} = v_0 \frac{\partial \rho^-}{\partial x} + \frac{1}{2}\Big(Z^+\rho^+ - Z^-\rho^-\Big), \tag{3.6}$$

$$\frac{\partial q^+}{\partial t} = -v_0 \frac{\partial q^+}{\partial x} + F^+\rho^+ - \frac{1}{2}\Big(Z^+q^+ - Z^-q^-\Big), \tag{3.7}$$

$$\frac{\partial q^-}{\partial t} = v_0 \frac{\partial q^-}{\partial x} + F^-\rho^- + \frac{1}{2}\Big(Z^+q^+ - Z^-q^-\Big). \tag{3.8}$$

Remark 2. The Taylor expansion in m gives a systematic way of constructing high order systems. For example, we can introduce two additional variables, $e^+(x,t) = \int (m - M^+)^2 P^+ \,\mathrm{d}m$ and $e^-(x,t) = \int (m - M^-)^2 P^- \,\mathrm{d}m$, and then construct a six-equation system by approximating

$$f(m) \approx f(m)|_{m=M^\pm} + \frac{\partial f}{\partial m}\Big|_{m=M^\pm}(m - M^\pm) + \frac{1}{2}\frac{\partial^2 f}{\partial m^2}\Big|_{m=M^\pm}(m - M^\pm)^2,$$

$$z(m) \approx z(m)|_{m=M^\pm} + \frac{\partial z}{\partial m}\Big|_{m=M^\pm}(m - M^\pm) + \frac{1}{2}\frac{\partial^2 z}{\partial m^2}\Big|_{m=M^\pm}(m - M^\pm)^2.$$

3.2. Numerical justification of Assumption A by SPECS. To justify Assumption A, we simulate the distribution of m using SPECS in an exponential gradient ligand environment $[L] = [L]_0 \exp(Gx)$. SPECS is a well-developed agent-based *E. coli* simulator that incorporates the physically measured signaling pathways and parameters [22]. In the simulation we introduced a "quasi-periodic" boundary condition: cells exiting at one side of the boundary will enter from the other side, and the methylation level is reset randomly following the local distribution of m at the boundaries. Using an exponential gradient ligand environment and this kind of boundary condition will lead to a well-defined distribution of the cells' methylation level. The steady state distributions are shown in Figure 1. In each of the subfigures, the horizontal and vertical axes represent the position and the methylation level, respectively. As shown in Figure 1, the distribution of cells' methylation level is localized and becomes wider when G increases. $M^\pm = \int mP^\pm \,\mathrm{d}m$ are the average methylation levels for the right- and left-moving cells. One can also observe that $M^+ < M^-$ in the exponential increasing ligand concentration environment. This can be understood intuitively by noticing that the up-gradient cells with lower methylation level come from the left, while the down-gradient cells with higher methylation level come from the right.

As shown in Figure 1, in an exponential gradient environment, the numerical variations in m appear almost uniform over all x. To test Assumption A, we check the maximum of the normalized variation of cells' methylation level,

$$\sigma \equiv \max \sqrt{\frac{\int \big(m/M(x) - 1\big)^2 (P^+ + P^-) dm}{\int (P^+ + P^-) dm}}, \quad \text{where} \quad M = \frac{\rho^+ M^+ + \rho^- M^-}{\rho^+ + \rho^-},$$

and also distinguish them by their moving directions:

$$\sigma^\pm \equiv \max \sqrt{\frac{\int \big(m/M^\pm(x) - 1\big)^2 P^\pm dm}{\int P^\pm dm}}.$$

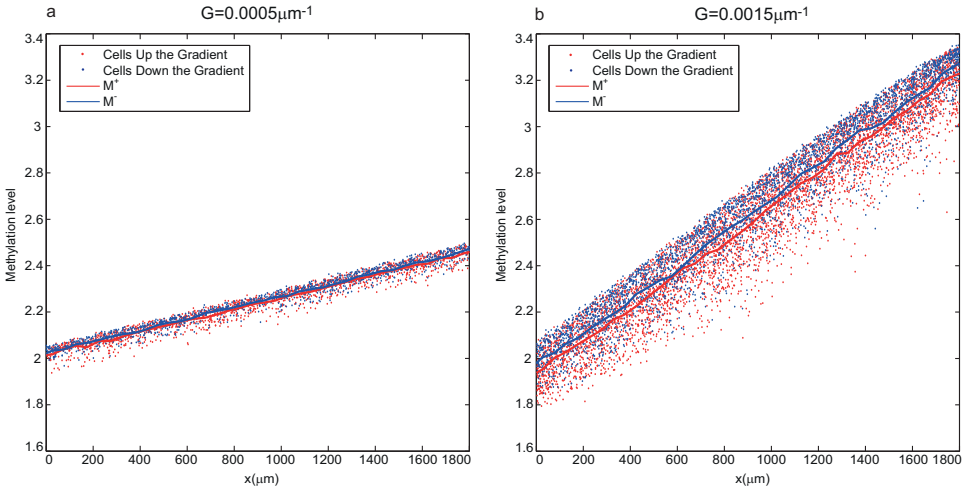

FIG. 1. *The distribution of cells' receptor methylation level in exponential gradient environment* $[L] = [L]_0 \exp(Gx)$. (a) $G = 0.0005\mu m^{-1}$ *and* (b) $G = 0.0015\mu m^{-1}$. *The red dots represent cells moving up the gradient (right side), while the blue ones represent those moving down the gradient (left side).* $M^{\pm}$ *are the average methylation levels for the right- and left-moving cells, respectively. In the simulation, we take* $[L]_0 = 5K_I$. *Other parameters are the same as those proposed in* [22].

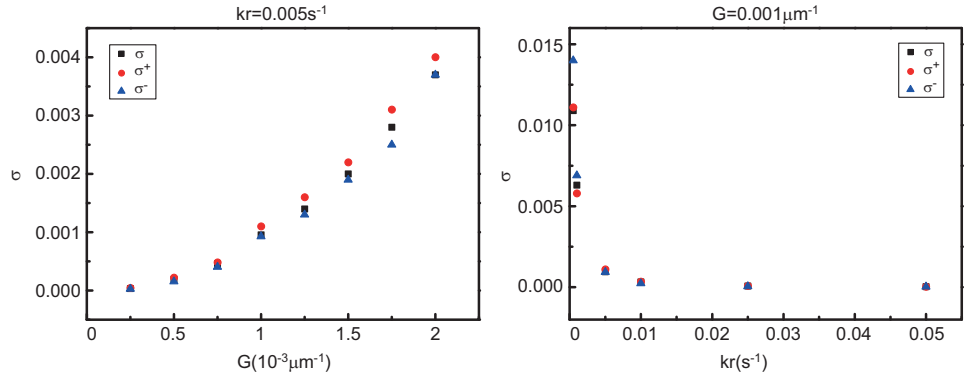

FIG. 2. *The variances of cells' methylation level for different* G *and* k_R. σ *is defined as the maximum of normalized variation of* m. $\sigma^{\pm}$ *are that of cells moving in "+" and "−" directions, respectively.* σ *and* $\sigma^{\pm}$ *increase with* G *for a given* k_R (a) *and decrease with* k_R *with fixed* G (b), *and their values are much smaller than* 1, *as demanded by Assumption* A.

As shown in Figure 2, both σ and $\sigma^{\pm}$ increase with G and decrease with k_R, and they are much smaller than 1; i.e., Assumption A holds in these cases.

3.3. The localization of $P^{\pm}$ in m in the limit of $k_R \gg 1$. We show by formal analysis that Assumption A is true when the adaptation rate $k_R \gg 1$. Denote

$$k_R = 1/\eta, \qquad f(a) = f_\eta(a)/\eta; \tag{3.9}$$

then (2.1)–(2.2) become

$$\frac{\partial P^+}{\partial t} = -\frac{\partial(v_0 P^+)}{\partial x} - \frac{1}{\eta}\frac{\partial(f_\eta(a)P^+)}{\partial m} - \frac{z}{2}(P^+ - P^-), \tag{3.10}$$

$$\frac{\partial P^-}{\partial t} = \frac{\partial(v_0 P^-)}{\partial x} - \frac{1}{\eta}\frac{\partial(f_\eta(a)P^-)}{\partial m} + \frac{z}{2}(P^+ - P^-). \tag{3.11}$$

Integrating the above two equations with respect to m produces, for $P_R^\pm(t,x) = \int_0^R P^\pm(t,x,m)\,dm$ (R is an arbitrary positive constant),

$$\begin{aligned}\frac{\partial P_R^+}{\partial t} = &-\frac{\partial(v_0 P_R^+)}{\partial x} - \frac{1}{2}\int_0^R z(P^+ - P^-)\,\mathrm{d}m \\ &- \frac{1}{\eta}f_\eta\big(a(R)\big)P^+(t,x,R) + \frac{1}{\eta}f_\eta\big(a(0)\big)P^+(t,x,0),\end{aligned} \tag{3.12}$$

$$\begin{aligned}\frac{\partial P_R^-}{\partial t} = &\frac{\partial(v_0 P_R^-)}{\partial x} + \frac{1}{2}\int_0^R z(P^+ - P^-)\,\mathrm{d}m \\ &- \frac{1}{\eta}f_\eta\big(a(R)\big)P^-(t,x,R) + \frac{1}{\eta}f_\eta\big(a(0)\big)P^-(t,x,0).\end{aligned} \tag{3.13}$$

The probability density functions satisfy $P^\pm(t,x,m) \geq 0\ \forall m \geq 0$, and thus $P_R^\pm(t,x)$ increases with R.

We consider the regime

$$\eta \ll 1, \quad \text{and} \quad f_\eta(a) \sim \mathcal{O}(1). \tag{3.14}$$

Then when $\eta \ll 1$, (3.12)+(3.13) indicate for $R \in (0,+\infty)$

$$f_\eta\big(a(R)\big)P^\pm(t,x,R) = f_\eta\big(a(0)\big)P^\pm(t,x,0) + O(\eta) = O(\eta), \tag{3.15}$$

where we have used the boundary condition that $P^\pm(t,x,m)$ decays to zero at $m = 0$.

Therefore, as $\eta \to 0$,

$$f_\eta(a(R))P^\pm(t,x,R) \to 0 \qquad \forall R \in (0,+\infty). \tag{3.16}$$

Then the definition of $f(a)$ in (2.3)–(2.4) gives that if $R \neq M_0$, $P^\pm(t,x,R) \to 0$, which implies that when $\eta \to 0$,

$$P^\pm(x,t,m) = \rho^\pm(x,t)\delta(m - M_{a0}), \tag{3.17}$$

where M_{a_0} is defined by $a([L](x,t), M_{a_0}(x,t)) = a_0$, which makes $f(a) = 0$.

Remark 3. When $\partial_t P_R^\pm$, $\partial_x P_R^\pm$ are $O(1)$, the locally concentrated property depends only on how large η is and not the magnitude of z. Therefore, the assumption that z is large in the derivation of parabolic and hyperbolic scaling in the subsequent section will not affect the locally concentrated property here. If the large gradient environment or the chemical signal changes too fast, $\partial_t P_R^\pm$, $\partial_x P_R^\pm$ become large, and the locally concentrated assumption is no longer true.

4. Connections to the original PBMFT and the KS limit. In this section, we connect the new moment system to the original PBMFT developed in [27] from (3.5)–(3.8) by taking into account the different physical time scales of the tumbling, adaptation, and experimental observations. In particular, one of the equations delivers

the important physical assumption equation (3) in [27]. We shall also derive the KS limit when the system time scale is longer. Moreover, a numerical comparison of the moment system (3.5)–(3.8) with SPECS is provided in the environment of spatial-temporally varying concentration.

We nondimensionalize the system (3.5)–(3.8) by letting

$$t = T\tilde{t}, \qquad x = L\tilde{x}, \qquad v_0 = s_0\tilde{v}_0,$$

where T and L are temporal and spatial scales of the system, respectively. Then the system becomes (after dropping the "$\sim$")

$$\begin{aligned}
\frac{1}{T}\frac{\partial \rho^+}{\partial t} &= -v_0\frac{\partial \rho^+}{\partial x}\frac{s_0}{L} - \frac{1}{2T_1}\Big(Z^+\rho^+ - Z^-\rho^-\Big),\\
\frac{1}{T}\frac{\partial \rho^-}{\partial t} &= v_0\frac{\partial \rho^-}{\partial x}\frac{s_0}{L} + \frac{1}{2T_1}\Big(Z^+\rho^+ - Z^-\rho^-\Big),\\
\frac{1}{T}\frac{\partial q^+}{\partial t} &= -v_0\frac{\partial q^+}{\partial x}\frac{s_0}{L} + \frac{1}{T_2}F^+\rho^+ - \frac{1}{2T_1}\Big(M^+Z^+\rho^+ - M^-Z^-\rho^-\Big),\\
\frac{1}{T}\frac{\partial q^-}{\partial t} &= v_0\frac{\partial q^-}{\partial x}\frac{s_0}{L} + \frac{1}{T_2}F^-\rho^- + \frac{1}{2T_1}\Big(M^+Z^+\rho^+ - M^-Z^-\rho^-\Big),
\end{aligned}$$

where T_1 and T_2 are the average run and adaptation time scales, respectively.

For *E. coli*, the average run time is on the order of 1s, the adaptation time is approximately 10s–100s, and, according to the experiment in [36], the system time scale when the PBMFT can be applied is all those scales longer than 80s, while the KS equation is only valid when the system time scale is longer than 1000s.

Therefore, for the PBMFT, we can consider the kinetic system (3.5)–(3.8) under the scaling (the so-called hyperbolic scaling) such that

$$\frac{T_1}{L/s_0} = \varepsilon, \quad \frac{T_2}{L/s_0} = 1, \quad \text{and} \quad \frac{T}{L/s_0} = 1 \tag{4.1}$$

with ε very small. On the other hand, for the KS equation in the longer time regime, we consider the parabolic scaling such that

$$\frac{T_1}{L/s_0} = \varepsilon, \quad \frac{T_2}{L/s_0} = 1, \quad \text{and} \quad \frac{T}{L/s_0} = \frac{1}{\varepsilon}. \tag{4.2}$$

In the subsequent part, when $\varepsilon \to 0$, we consider the Hilbert expansions

$$\begin{aligned}
&\rho^\pm = \rho^{\pm(0)} + \varepsilon\rho^{\pm(1)} + \cdots, \qquad q^\pm = q^{\pm(0)} + \varepsilon q^{\pm(1)} + \cdots,\\
&M^\pm = M^{\pm(0)} + \varepsilon M^{\pm(1)} + \cdots, \qquad F^\pm = F^{\pm(0)} + \varepsilon F^{\pm(1)} + \cdots,\\
&Z^\pm = Z^{\pm(0)} + \varepsilon Z^{\pm(1)} + \cdots
\end{aligned} \tag{4.3}$$

and use asymptotic analysis to connect (3.5)–(3.8) to both the PBMFT and the KS equation.

4.1. The original PBMFT by the hyperbolic scaling. The macroscopic quantities in the PBMFT in [27] are the total density ρ_s, the cell flux J_s, the average methylation M_s, and the methylation difference ΔM_s. M^+, M^- are the average methylation levels to the right and to the left. The connections of (3.1), (3.2) to the

macroscopic quantities in PBMFT are

(4.4)
$$\rho_s = \rho^+ + \rho^-, \qquad J_s = v_0(\rho^+ - \rho^-),$$
$$\Delta M_s = \frac{1}{2}(M^+ - M^-) = \frac{1}{2}\left(\frac{q^+}{\rho^+} - \frac{q^-}{\rho^-}\right), \qquad M_s = \frac{M^+\rho^+ + M^-\rho^-}{\rho^+ + \rho^-} = \frac{q^+ + q^-}{\rho^+ + \rho^-}.$$

The model in [27] is

$$\frac{\partial \rho_s}{\partial t} = -\frac{\partial J_s}{\partial x}, \tag{4.5}$$

$$J_s = -v_0^2 Z_s^{-1}\frac{\partial \rho_s}{\partial x} - v_0 Z_s^{-1}\frac{\partial Z_s}{\partial m}\Delta M_s \rho_s, \tag{4.6}$$

$$\frac{\partial M_s}{\partial t} \approx F_s - \frac{J_s}{\rho_s}\frac{\partial M_s}{\partial x} - \frac{1}{\rho_s}\frac{\partial}{\partial x}(v_0 \Delta M_s \rho_s), \tag{4.7}$$

together with the physical assumption

$$\Delta M_s \approx -\frac{\partial M_s}{\partial x} Z_s^{-1} v_0, \tag{4.8}$$

which physically means that ΔM_s is approximated by the methylation level difference in the mean methylation field $M_s(x,t)$ over the average run length $v_0 Z^{-1}$ due to the fact that the direction of motion is randomized during each tumble event. Here

$$Z_s = z(M_s), \qquad F_s = f(M_s).$$

Under the scaling (4.1), (3.5)–(3.8) become

$$\frac{\partial \rho^+}{\partial t} = -v_0\frac{\partial \rho^+}{\partial x} - \frac{1}{2\varepsilon}\Big(Z^+\rho^+ - Z^-\rho^-\Big), \tag{4.9}$$

$$\frac{\partial \rho^-}{\partial t} = v_0\frac{\partial \rho^-}{\partial x} + \frac{1}{2\varepsilon}\Big(Z^+\rho^+ - Z^-\rho^-\Big), \tag{4.10}$$

$$\frac{\partial q^+}{\partial t} = -v_0\frac{\partial q^+}{\partial x} + F^+\rho^+ - \frac{1}{2\varepsilon}\Big(M^+Z^+\rho^+ - M^-Z^-\rho^-\Big), \tag{4.11}$$

$$\frac{\partial q^-}{\partial t} = v_0\frac{\partial q^-}{\partial x} + F^-\rho^- + \frac{1}{2\varepsilon}\Big(M^+Z^+\rho^+ - M^-Z^-\rho^-\Big). \tag{4.12}$$

Introducing the asymptotic expansions as in (4.3), we first look at those leading order terms. Matching the $O(1/\varepsilon)$ terms in (4.10) and (4.12) gives

$$Z^{+(0)}\rho^{+(0)} = Z^{-(0)}\rho^{-(0)} \quad \text{and} \quad M^{+(0)}Z^{+(0)}\rho^{+(0)} = M^{+(0)}Z^{-(0)}\rho^{-(0)},$$

which implies

$$M^{+(0)} = M^{-(0)}.$$

Since $z(a)$, $f(a)$ are continuous functions of m, $Z^{+(0)} = Z^{-(0)}$, $F^{+(0)} = F^{-(0)}$. Then $Z^{+(0)}\rho^{+(0)} = Z^{-(0)}\rho^{-(0)}$ indicates that $\rho^{+(0)} = \rho^{-(0)}$ and $q^{+(0)} = M^{+(0)}\rho^{+(0)} = M^{-(0)}\rho^{-(0)} = q^{-(0)}$. For simplicity, in the following, we denote

$$\begin{aligned} &\rho_0 = \rho^{\pm(0)}, \quad M_0 = M^{\pm(0)}, \quad q_0 = q^{\pm(0)}, \\ &Z_0 = Z^{\pm(0)}, \quad F_0 = F^{\pm(0)}, \quad \frac{\partial Z_0}{\partial m} = \frac{\partial z}{\partial m}\Big|_{m=M^{\pm(0)}}. \end{aligned} \tag{4.13}$$

On the other hand, let

$$\rho_s = \rho_s^{(0)} + \varepsilon\rho_s^{(1)} + \cdots, \qquad J_s = J_s^{(0)} + \varepsilon J_s^{(1)} + \cdots,$$
$$\Delta M_s = \Delta M_s^{(0)} + \varepsilon\Delta M_s^{(1)} + \cdots, \qquad M_s = M_s^{(0)} + \varepsilon M_s^{(1)} + \cdots.$$

Then the connections of the macroscopic quantities give

(4.14)
$$\rho_s^{(0)} = 2\rho_0, \qquad J_s^{(0)} = 0, \qquad \Delta M_s^{(0)} = 0, \qquad M_s^{(0)} = M_0,$$
$$\rho_s^{(1)} = \rho^{+(1)} + \rho^{-(1)}, \qquad J_s^{(1)} = v_0\big(\rho^{+(1)} - \rho^{-(1)}\big), \qquad \Delta M_s^{(1)} = \frac{1}{2}\big(M^{+(1)} - M^{-(1)}\big).$$

Moreover, it is important to note that we have dropped the "$\sim$" in the rescaled system (4.9)–(4.12); therefore, $Z = z(M_s)$ in (4.5)–(4.8) is

$$Z_s = z(M_0 + \varepsilon M_s^{(1)} + \cdots) = z(M_0) + O(\varepsilon) = \frac{\tilde{z}(M_0) + O(\varepsilon)}{\varepsilon} = \frac{Z_0}{\varepsilon} + O(1). \tag{4.15}$$

In the following, we derive (4.5)–(4.8) by asymptotics:

- Adding (4.9) and (4.10) brings (4.5).
- Subtracting (4.9) by (4.10) gives

$$\frac{\partial J_s}{\partial t} = -v_0^2\frac{\partial \rho_s}{\partial x} - \frac{v_0}{\varepsilon}\big(Z^+\rho^+ - Z^-\rho^-\big).$$

Since

$$\begin{aligned} Z^\pm &= z(M^\pm, [L]) = z\big(M^{\pm(0)} + \varepsilon M^{\pm(1)} + \cdots, [L]\big) \\ &= z(M_0, [L]) + \varepsilon\frac{\partial z}{\partial m}\Big|_{m=M_0} M^{\pm(1)} + \cdots = Z_0 + \varepsilon\frac{\partial Z_0}{\partial m}M^{\pm(1)} + \cdots, \end{aligned}$$

we find

$$Z^{+(1)} - Z^{-(1)} = \frac{\partial Z_0}{\partial m}\big(M^{+(1)} - M^{-(1)}\big). \tag{4.16}$$

Then $O(1)$ terms of subtracting (4.9) by (4.10) yield

(4.17)
$$\begin{aligned} \frac{\partial J_s^{(0)}}{\partial t} &= -v_0^2\frac{\partial \rho_s^{(0)}}{\partial x} - v_0\big(Z^{+(0)}\rho^{+(1)} - Z^{-(0)}\rho^{-(1)}\big) - v_0\big(Z^{+(1)}\rho^{+(0)} - Z^{-(1)}\rho^{-(0)}\big) \\ &= -v_0^2\frac{\partial \rho_s^{(0)}}{\partial x} - Z_0 v_0\big(\rho^{+(1)} - \rho^{-(1)}\big) - \rho_0 v_0\frac{\partial Z_0}{\partial m}\big(M^{+(1)} - M^{-(1)}\big) \\ &= -v_0^2\frac{\partial \rho_s^{(0)}}{\partial x} - Z_0 J_s^{(1)} - \rho_s^{(0)} v_0\frac{\partial Z_0}{\partial m}\Delta M_s^{(1)} \\ &= -v_0^2\frac{\partial \rho_s^{(0)}}{\partial x} - Z_s J_s - v_0\frac{\partial Z_s}{\partial m}\Delta M_s\rho_s^{(0)} + O(\varepsilon). \end{aligned}$$

Here, in the first equation, we have used (4.16). In the last two equations, we have used (4.14), (4.15), and the result is accurate to $O(\varepsilon)$.

Then, from $J_s^{(0)} = 0$,

$$-v_0^2\frac{\partial \rho_s^{(0)}}{\partial x} - Z_s J_s - v_0\frac{\partial Z_s}{\partial m}\Delta M_s\rho_s^{(0)} = 0,$$

and we get (4.6).

- Adding (4.11) and (4.12) gives

$$\frac{\partial\big(q^+ + q^-\big)}{\partial t} = -v_0\frac{\partial\big(q^+ - q^-\big)}{\partial x} + F^+\rho^+ + F^-\rho^-. \tag{4.18}$$

From (4.14), (4.4), we have

$$\begin{aligned} v_0(q^+ - q^-) &= v_0(\rho^+M^+ - \rho^-M^-) \\ &= \varepsilon M_0 v_0\big(\rho^{+(1)} - \rho^{-(1)}\big) + \varepsilon\rho_0 v_0\big(M^{+(1)} - M^{-(1)}\big) + O(\varepsilon^2) \\ &= M_s J_s + \rho_s v_0 \Delta M_s + O(\varepsilon^2), \end{aligned}$$

and

$$\begin{aligned} F^+\rho^+ + F^-\rho^- &= f(M^+)\rho^+ + f(M^-)\rho^- \\ &= f\big(M_s + (M^+ - M_s)\big)\rho^+ + f\big(M_s + (M^- - M_s)\big)\rho^- \\ &= F_s\rho_s + \frac{\partial f}{\partial m}\Big|_{m=M_s}\Big((M^+ - M_s)\rho^+ + (M^- - M_s)\rho^-\Big) + O(\varepsilon^2) \\ &= F_s\rho_s + O(\varepsilon^2). \end{aligned}$$

Therefore, (4.18) is equivalent to

$$\begin{aligned} \frac{\partial\big(M_s\rho_s\big)}{\partial t} &= -v_0\frac{\partial\big(\rho_s\Delta M_s\big)}{\partial x} - \frac{\partial\big(M_s J_s\big)}{\partial x} + F_s\rho_s + O(\varepsilon^2) \\ &= -v_0\frac{\partial(\rho_s\Delta M_s)}{\partial x} - M_s\frac{\partial J_s}{\partial x} - J_s\frac{\partial M_s}{\partial x} + F_s\rho_s + O(\varepsilon^2). \end{aligned}$$

By using (4.5), the above equation is the same as (4.7), and it is accurate up to $O(\varepsilon^2)$.

- Finally, from (4.13), the $O(1)$ terms of subtracting (4.11) by (4.12) yield

$$-2v_0\frac{\partial q_0}{\partial x} - \Big(Z_0\big(M^{+(1)} - M^{-(1)}\big) + M_0\big(Z^{+(1)} - Z^{-(1)}\big)\Big)\rho_0 - M_0 Z_0\big(\rho^{+(1)} - \rho^{-(1)}\big) = 0.$$

Noting the first equation in (4.17), the above equation is equivalent to

$$M_0 v_0^{-1}\frac{\partial J_s^{(0)}}{\partial t} - 2v_0\rho_0\frac{\partial M_0}{\partial x} - 2Z_0\Delta M_s^{(1)}\rho_0 = 0.$$

Thanks to $J_s^{(0)} = 0$, $\Delta M_s^{(0)} = 0$ from (4.14), and the relation of Z and Z_0 in (4.15), the above equation leads to the important physical assumption (4.8),

$$\Delta M_s \approx -\frac{\partial M_0}{\partial x} Z^{-1} v_0. \tag{4.19}$$

We have recovered the PBMFT model in [27].

Remark 4. In the derivation of the PBMFT, we have decomposed the tumbling frequency into two different scales. This idea is similar to the general derivation approach in [17], but we have additional equations for the time evolution of the methylation level. Since the turning operator depends on the methylation level, which also changes dynamically, it is hard to determine explicitly how the turning operator depends on $[L]$ as in [17]. According to [17], the Hilbert approach indicates that the PBMFT is an approximation of order ε of the transport system (3.5)–(3.8), which is not clear for the moment system in [15, 16, 35].

4.2. KS limit by the parabolic scaling. Under the scaling (4.2), (3.5)–(3.8) become

$$\varepsilon\frac{\partial\rho^+}{\partial t} = -v_0\frac{\partial\rho^+}{\partial x} - \frac{1}{2\varepsilon}\Big(Z^+\rho^+ - Z^-\rho^-\Big), \tag{4.20}$$

$$\varepsilon\frac{\partial\rho^-}{\partial t} = v_0\frac{\partial\rho^-}{\partial x} + \frac{1}{2\varepsilon}\Big(Z^+\rho^+ - Z^-\rho^-\Big), \tag{4.21}$$

$$\varepsilon\frac{\partial q^+}{\partial t} = -v_0\frac{\partial q^+}{\partial x} + F^+\rho^+ - \frac{1}{2\varepsilon}\Big(M^+Z^+\rho^+ - M^-Z^-\rho^-\Big), \tag{4.22}$$

$$\varepsilon\frac{\partial q^-}{\partial t} = v_0\frac{\partial q^-}{\partial x} + F^-\rho^- + \frac{1}{2\varepsilon}\Big(M^+Z^+\rho^+ - M^-Z^-\rho^-\Big). \tag{4.23}$$

First, we have equations similar to those in (4.13). Additionally, the $O(1)$ terms in (4.22)+(4.23) and (4.13) yield $F^{\pm(0)} = 0$, which is the main difference between the hyperbolic and parabolic scalings. Then equating the $O(\varepsilon)$ terms in adding (4.20) and (4.21) together produces

$$2\frac{\partial\rho_0}{\partial t} = -v_0\frac{\partial\big(\rho^{+(1)} - \rho^{-(1)}\big)}{\partial x}. \tag{4.24}$$

Putting together the $O(1)$ terms in subtracting (4.20) by (4.21) and subtracting (4.22) by (4.23) brings about

$$-2v_0\frac{\partial\rho_0}{\partial x} - Z_0\big(\rho^{+(1)} - \rho^{-(1)}\big) - \rho_0\big(Z^{+(1)} - Z^{-(1)}\big) = 0, \tag{4.25}$$

$$\begin{aligned} &-v_0\frac{\partial\big(q^{+(0)} + q^{-(0)}\big)}{\partial x} - M_0Z_0\big(\rho^{+(1)} - \rho^{-(1)}\big) \\ &\qquad - \Big(Z_0\big(M^{+(1)} - M^{-(1)}\big) + M_0\big(Z^{+(1)} - Z^{-(1)}\big)\Big)\rho_0 = 0. \end{aligned} \tag{4.26}$$

Multiplying (4.25) by M_0 and subtracting it from (4.26) give

$$-2v_0\rho_0\frac{\partial M_0}{\partial x} - Z_0\rho_0\big(M^{+(1)} - M^{-(1)}\big) = 0.$$

Then, from (4.16), the two equations (4.25) and (4.26) imply

$$\begin{aligned} \rho^{+(1)} - \rho^{-(1)} &= Z_0^{-1}\bigg(-2v_0\frac{\partial\rho_0}{\partial x} - \frac{\partial Z_0}{\partial m}\big(M^{+(1)} - M^{-(1)}\big)\rho_0\bigg) \\ &= Z_0^{-1}\bigg(-2v_0\frac{\partial\rho_0}{\partial x} + 2v_0Z_0^{-1}\frac{\partial Z_0}{\partial m}\frac{\partial M_0}{\partial x}\rho_0\bigg) \\ &= -2v_0Z_0^{-1}\frac{\partial\rho_0}{\partial x} + 2v_0Z_0^{-2}\frac{\partial Z_0}{\partial m}\frac{\partial M_0}{\partial x}\rho_0. \end{aligned} \tag{4.27}$$

Substituting (4.27) into (4.24) gives the KS equation

$$\frac{\partial\rho^{(0)}}{\partial t} = v_0^2\frac{\partial}{\partial x}\bigg(Z_0^{-1}\frac{\partial\rho^{(0)}}{\partial x}\bigg) - v_0^2\frac{\partial}{\partial x}\bigg(Z_0^{-2}\frac{\partial Z_0}{\partial m}\frac{\partial M_0}{\partial x}\rho^{(0)}\bigg). \tag{4.28}$$

Using $M_0 = M_{a_0}$, $Z_0 = z(M_{a_0})$, the latter equation becomes

$$\frac{\partial\rho^{(0)}}{\partial t} = v_0^2\frac{\partial}{\partial x}\Big(Z_0^{-1}\frac{\partial\rho^{(0)}}{\partial x}\Big) - \frac{\partial}{\partial x}\Big(\chi_0\rho^{(0)}\frac{\partial f_0}{\partial x}\Big) \tag{4.29}$$

with $\chi_0 = \dfrac{v_0^2\tau^{-1}}{(z_0+\tau^{-1})^2}NH(1-a_0)$.

Remark 5. 1. If instead of (4.2), we consider

$$\frac{T_1}{L/s_0} = \varepsilon, \quad \frac{T_2}{L/s_0} = \kappa\varepsilon, \quad \text{and} \quad \frac{T}{L/s_0} = \frac{1}{\varepsilon},$$

then the rescaled system becomes

$$\begin{aligned}
\varepsilon\frac{\partial\rho^+}{\partial t} &= -v_0\frac{\partial\rho^+}{\partial x} - \frac{1}{2\varepsilon}\Big(Z^+\rho^+ - Z^-\rho^-\Big),\\
\varepsilon\frac{\partial\rho^-}{\partial t} &= v_0\frac{\partial\rho^-}{\partial x} + \frac{1}{2\varepsilon}\Big(Z^+\rho^+ - Z^-\rho^-\Big),\\
\varepsilon\frac{\partial q^+}{\partial t} &= -v_0\frac{\partial q^+}{\partial x} + \frac{1}{\kappa\varepsilon}F^+\rho^+ - \frac{1}{2\varepsilon}\Big(M^+Z^+\rho^+ - M^-Z^-\rho^-\Big),\\
\varepsilon\frac{\partial q^-}{\partial t} &= v_0\frac{\partial q^-}{\partial x} + \frac{1}{\kappa\varepsilon}F^-\rho^- + \frac{1}{2\varepsilon}\Big(M^+Z^+\rho^+ - M^-Z^-\rho^-\Big).
\end{aligned}$$

When $\kappa \le O(1/\varepsilon)$, carrying on a similar asymptotic expansion will produce the same KS limit (4.29) as $\epsilon \to 0$. This indicates that when the adaptation time is shorter than $\sqrt{TT_1}$, the KS equation is valid for *E. coli* chemotaxis.

2. The velocity scale of individual bacteria is s_0. The temporal and spatial scales of the system we consider are T and L, respectively; therefore, the velocity scale of the drift velocity $v_d = J_\rho/\rho$ is L/T. The scaling (4.2) implies $v_d/s_0 \sim O(\varepsilon)$, which means that in the regime where KS equation is valid, the drift velocity is much smaller than the moving velocity of individual bacteria.

3. If the adaptation is faster than the characteristic tumbling time, which indicates that *E. coli* can adapt to the environment almost immediately, it exhibits no chemotactic behavior since the tumbling frequencies are the same in different directions.

4.3. Numerical comparison in the traveling wave concentration. To show the validity of the moment system (3.5)–(3.8), numerical comparisons to SPECS will be presented in this subsection. We choose the spatial-temporal varying environment to show how the intracellular dynamics affects the *E. coli* behaviors at the population level.

We consider a periodic one-dimensional domain with the traveling wave concentration given by $[L](x,t) = [L]_0 + [L]_A + \sin[\frac{2\pi}{\lambda}(x-ut)]$. The wavelength λ is fixed to be the length of the domain, while the wave velocity u can be tuned. The traveling wave profiles of all the macroscopic quantities in (3.5)–(3.8) and corresponding SPECS results are compared in Figure 3. The results from SPECS and the moment system are quantitatively consistent. It can be noticed that, when the concentration changes slowly ($u = 0.4\mu m/s$), the profile of M can catch up with the target value M_{a_0} (defined by $a([L], M_{a_0}) = a_0$), while in the fast-varying environment ($u = 8\mu m/s$) there is a lag in phase between M and M_{a_0}. This difference is caused by the slow adaptation rate of cells, and it also leads to the difference in the profiles of ρ and even chemotactic velocity; we refer interested readers to [27] for more detailed discussions and physical explanations.

5. Two-dimensional mean-field model. In this section, we derive the two-dimensional moment system of PBMFT based on a formal argument using the point-mass assumption in methylation and the minimization principle proposed in [20].

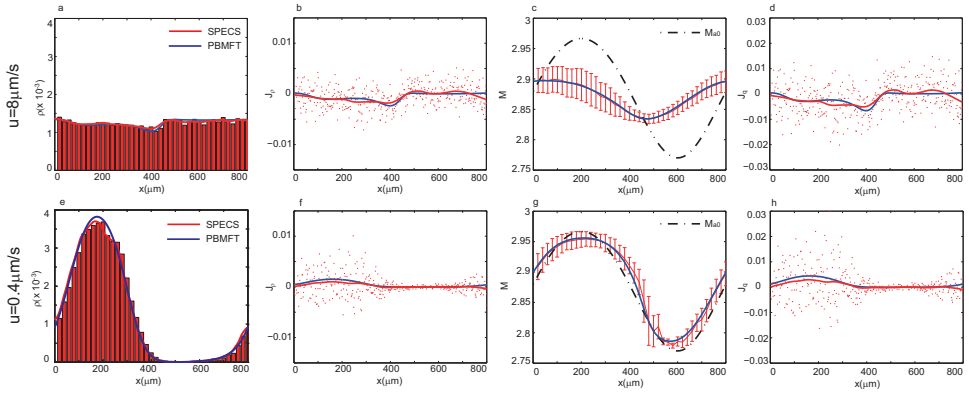

FIG. 3. *Numerical comparison between the new transport system and SPECS. The steady state profiles of* ρ*:* (a), (e)*;* J_ρ*:* (b), (f)*;* $M = q/\rho$*:* (c), (g)*;* J_q*:* (d), (h) *when the traveling wave speeds are* $u = 8\mu m/s$ *and* $u = 0.4\mu m/s$*, respectively. In the subfigures, red lines, histograms, and dots are from SPECS (red lines in* (a) *and* (e) *are the estimated probability densities of the red histograms; red lines in* (b), (d), (f), (h) *are the smoothed results of the red dots), while blue lines are calculated using the new transport system of PBMFT. Parameters used here are* $[L]_0 = 500\mu M$*,* $[L]_A = 100\mu M$*,* $\lambda = 800\mu m$*. 20000 cells are simulated in SPECS.*

In two dimensions, $\boldsymbol{v} = v_0(\cos\theta, \sin\theta)$, where v_0 is the velocity magnitude. $P(t, \boldsymbol{x}, \boldsymbol{v}, m)$ in (2.7) can be rewritten as $P(t, \boldsymbol{x}, \theta, m)$. $z(m, [L], \theta, \theta')$ is the tumbling rate from θ' to θ. The tumbling term $Q(P, z)$ in (2.8) becomes

(5.1)
$$Q(P,z) = \fint_V z(m,[L],\theta,\theta')P(t,\boldsymbol{x},\theta',m)\,\mathrm{d}\theta' - \fint_V z(m,[L],\theta',\theta)\,\mathrm{d}\theta' P(t,\boldsymbol{x},\theta,m),$$

where $V = [0, 2\pi)$ and $\fint = \frac{1}{2\pi}\int_V$. According to (2.6), $z(m, [L], \theta, \theta')$ is independent of θ, and thus we denote it by $z(m, [L])$.

Define

(5.2)
$$g(t,\boldsymbol{x},\theta) = \int P(t,\boldsymbol{x},\theta,m)\,\mathrm{d}m, \qquad h(t,\boldsymbol{x},\theta) = \int mP(t,\boldsymbol{x},\theta,m)\,\mathrm{d}m,$$

(5.3)
$$M(t,\boldsymbol{x},\theta) = \frac{h(t,\boldsymbol{x},\theta)}{g(t,\boldsymbol{x},\theta)},$$

and the density and momentum (in m) as

(5.4)
$$\begin{aligned}
\rho^f(t,\boldsymbol{x}) &= \fint_{V_f} g(t,\boldsymbol{x},\theta)\,\mathrm{d}\theta, \quad \rho^b(t,\boldsymbol{x}) = \fint_{V_b} \boldsymbol{v}g(t,\boldsymbol{x},\theta)\,\mathrm{d}\theta,\\
\rho^u(t,\boldsymbol{x}) &= \fint_{V_u} g(t,\boldsymbol{x},\theta)\,\mathrm{d}\theta, \quad \rho^d(t,\boldsymbol{x}) = \fint_{V_d} \boldsymbol{v}g(t,\boldsymbol{x},\theta)\,\mathrm{d}\theta,\\
q^f(t,\boldsymbol{x}) &= \fint_{V_f} h(t,\boldsymbol{x},\theta)\,\mathrm{d}\theta, \quad q^b(t,\boldsymbol{x}) = \fint_{V_b} \boldsymbol{v}h(t,\boldsymbol{x},\theta)\,\mathrm{d}\theta,\\
q^u(t,\boldsymbol{x}) &= \fint_{V_u} h(t,\boldsymbol{x},\theta)\,\mathrm{d}\theta, \quad q^d(t,\boldsymbol{x}) = \fint_{V_d} \boldsymbol{v}h(t,\boldsymbol{x},\theta)\,\mathrm{d}\theta,
\end{aligned}$$

where $\fint = \frac{2}{\pi}\int$ and

$$V_f = (7\pi/4, 0)\cup[0, \pi/4), \quad V_b = (3\pi/4, 5\pi/4), \quad V_u = (\pi/4, 3\pi/4), \quad V_d = (5\pi/4, 7\pi/4).$$

We assume

$$P(t,\boldsymbol{x},\theta,m) = g(t,\boldsymbol{x},\theta)\delta\big(m - M(t,\boldsymbol{x},\theta)\big). \tag{5.5}$$

This assumption is motivated by (3.17) in one dimension, which could be formally understood as the limit of $k_R \to +\infty$.

Let i represent all four possible superscripts f, b, u, d, and denote

$$M^i = \frac{q^i}{\rho^i}, \quad Z^i = z(M^i), \quad \frac{\partial Z^i}{\partial m} = \frac{\partial z}{\partial m}(M^i), \quad F^i = f(M^i), \quad \frac{\partial F^i}{\partial m} = \frac{\partial f}{\partial m}(M^i). \tag{5.6}$$

Integrating (2.7) with respect to m yields

$$\partial_t g = -\boldsymbol{v}\cdot\nabla_{\boldsymbol{x}} g + \fint_V z\big(M(\theta'),[L]\big)g(t,\boldsymbol{x},\theta')\,\mathrm{d}\theta' - z\big(M(\theta),[L]\big)g(t,\boldsymbol{x},\theta). \tag{5.7}$$

Integrating (5.7) with respect to θ from $7\pi/4$ to 2π and 0 to $\pi/4$ gives the equation for ρ^f,

$$\begin{aligned}\frac{\partial \rho^f(t,\boldsymbol{x})}{\partial t} \approx & -\fint_{V_f} \boldsymbol{v}\cdot\nabla_{\boldsymbol{x}} g\,\mathrm{d}\theta - \frac{3}{4}\fint_{V_f}\Big(Z^f + \frac{\partial Z^f}{\partial m}(M-M^f)\Big)g\,\mathrm{d}\theta \\ & + \frac{1}{4}\fint_{V_b}\Big(Z^b + \frac{\partial Z^b}{\partial m}(M-M^b)\Big)g\,\mathrm{d}\theta + \frac{1}{4}\fint_{V_u}\Big(Z^u + \frac{\partial Z^u}{\partial m}(M-M^u)\Big)g\,\mathrm{d}\theta \\ & + \frac{1}{4}\fint_{V_d}\Big(Z^d + \frac{\partial Z^f}{\partial m}(M-M^d)\Big)g\,\mathrm{d}\theta \\ = & -\fint_{V_f}\boldsymbol{v}\cdot\nabla_{\boldsymbol{x}} g\,\mathrm{d}\theta - \frac{3}{4}Z^f\rho^f + \frac{1}{4}Z^b\rho^b + \frac{1}{4}Z^u\rho^u + \frac{1}{4}Z^d\rho^d.\end{aligned} \tag{5.8}$$

Similar equations can be found for ρ^b, ρ^u, ρ^d, but we exchange the superscript f with b, u, and d, respectively.

Multiplying (2.7) by m and integrating it with respect to m bring about

$$\begin{aligned}\partial_t h = -\boldsymbol{v}\cdot\nabla_{\boldsymbol{x}} h + f\big(M(\theta),[L]\big)g(\theta) + \fint_V z\big(M(\theta'),[L]\big)g(\theta')M(\theta')\,\mathrm{d}\theta' \\ - z(M(\theta),[L])g(\theta)M(\theta).\end{aligned} \tag{5.9}$$

Integrating (5.9) with respect to θ from $7\pi/4$ to 2π and 0 to $\pi/4$ and using the

definition in (5.3) give

$$
\begin{aligned}
\frac{\partial q^f(\boldsymbol{x},t)}{\partial t} \approx & -\fint_{V_f} \boldsymbol{v}\cdot\nabla_{\boldsymbol{x}} h\,\mathrm{d}\theta + \fint_{V_f}\Big(F^f + \frac{\partial F^f}{\partial m}(M-M^f)\Big)g(\boldsymbol{x},t,\theta)\,\mathrm{d}\theta \\
& -\frac{3}{4}\fint_{V_f}\Big(Z^f M^f + \Big(Z^f + M^f\frac{\partial Z^f}{\partial m}\Big)\big(M-M^f\big)\Big)g\,\mathrm{d}\theta \\
& +\frac{1}{4}\fint_{V_b}\Big(Z^b M^b + \Big(Z^b + M^b\frac{\partial Z^b}{\partial m}\Big)\big(M-M^b\big)\Big)g\,\mathrm{d}\theta \\
& +\frac{1}{4}\fint_{V_u}\Big(Z^u M^u + \Big(Z^u + M^u\frac{\partial Z^u}{\partial m}\Big)\big(M-M^u\big)\Big)g\,\mathrm{d}\theta \\
& +\frac{1}{4}\fint_{V_d}\Big(Z^d M^d + \Big(Z^d + M^d\frac{\partial Z^d}{\partial m}\Big)\big(M-M^d\big)\Big)g\,\mathrm{d}\theta \\
= & -\fint_{V_f}\boldsymbol{v}\cdot\nabla_{\boldsymbol{x}} h\,\mathrm{d}\theta + F^f\rho^f - \frac{3}{4}Z^f q^f + \frac{1}{4}Z^b q^b + \frac{1}{4}Z^u q^u + \frac{1}{4}Z^d q^d.
\end{aligned}
\tag{5.10}
$$

Similar equations can be found for q^b, q^u, q^d, but we exchange the superscript f with b, u, and d, respectively.

In order to close the system, we need a constitutive relation that represents $-\fint_{V_i}\boldsymbol{v}\cdot\nabla_{\boldsymbol{x}} g\,\mathrm{d}\theta$ and $-\fint_{V_i}\boldsymbol{v}\cdot\nabla_{\boldsymbol{x}} h\,\mathrm{d}\theta$ by ρ^i, q^i (i represents f, b, u, d). Assume

$$
\begin{aligned}
g(t,\boldsymbol{x},\theta) &\approx g_1(t,\boldsymbol{x}) + \tfrac{\pi}{2}g_c(t,\boldsymbol{x})\cos\theta + \tfrac{\pi}{2}g_s(t,\boldsymbol{x})\sin\theta + \tfrac{\pi}{2}g_{2c}(t,\boldsymbol{x})\cos 2\theta,\\
h(t,\boldsymbol{x},\theta) &\approx h_1(t,\boldsymbol{x}) + \tfrac{\pi}{2}h_c(t,\boldsymbol{x})\cos\theta + \tfrac{\pi}{2}h_s(t,\boldsymbol{x})\sin\theta + \tfrac{\pi}{2}h_{2c}(t,\boldsymbol{x})\cos 2\theta.
\end{aligned}
\tag{5.11}
$$

Then from (5.4),

$$
\begin{aligned}
\rho^f(t,\boldsymbol{x}) &\approx \fint_{V_f} g(t,\boldsymbol{x},\theta)\,\mathrm{d}\theta = g_1 + \sqrt{2}g_c + g_{2c},\\
q^f(t,\boldsymbol{x}) &\approx \fint_{V_f} h(t,\boldsymbol{x},\theta)\,\mathrm{d}\theta = h_1 + \sqrt{2}h_c + h_{2c}.
\end{aligned}
$$

Similarly,

$$
\begin{aligned}
&\rho^b \approx g_1 - \sqrt{2}g_c + g_{2c},\quad \rho^u \approx g_1 + \sqrt{2}g_s - g_{2c},\quad \rho^d = g_1 - \sqrt{2}g_s - g_{2c},\\
&q^b \approx h_1 - \sqrt{2}h_c + h_{2c},\quad q^u \approx h_1 + \sqrt{2}h_s - h_{2c},\quad q^d = h_1 - \sqrt{2}h_s - h_{2c}.
\end{aligned}
$$

Therefore, expressing g_1, g_c, g_s, g_{2c}, h_1, h_c, h_s, h_{2c} by ρ^f, ρ^b, ρ^u, ρ_d, q^f, q^b, q^u, q_d, we find

$$
\begin{aligned}
g_1 &= \frac{1}{4}\big(\rho^f + \rho^b + \rho^u + \rho^d\big), \qquad g_{2c} = \frac{1}{4}\big(\rho^f + \rho^b - \rho^u - \rho^d\big),\\
g_c &= \frac{\sqrt{2}}{4}\big(\rho^f - \rho^b\big), \qquad g_s = \frac{\sqrt{2}}{4}\big(\rho^u - \rho^d\big),\\
h_1 &= \frac{1}{4}\big(q^f + q^b + q^u + q^d\big), \qquad h_{2c} = \frac{1}{4}\big(q^f + q^b - q^u - q^d\big),\\
h_c &= \frac{\sqrt{2}}{4}\big(q^f - q^b\big), \qquad h_s = \frac{\sqrt{2}}{4}\big(q^u - q^d\big).
\end{aligned}
\tag{5.12}
$$

Hence,

$$
\begin{aligned}
&\fint_{V_f} \boldsymbol{v}\cdot\nabla_{\boldsymbol{x}} g\,\mathrm{d}\theta \approx \frac{2\sqrt{2}}{\pi}\partial_x g_1 + \Big(\frac{\pi}{4}+\frac{1}{2}\Big)\partial_x g_c + \Big(\frac{\pi}{4}-\frac{1}{2}\Big)\partial_y g_s + \frac{2\sqrt{2}}{3}\partial_x g_{2c},\\
&\fint_{V_b} \boldsymbol{v}\cdot\nabla_{\boldsymbol{x}} g\,\mathrm{d}\theta \approx -\frac{2\sqrt{2}}{\pi}\partial_x g_1 + \Big(\frac{\pi}{4}+\frac{1}{2}\Big)\partial_x g_c + \Big(\frac{\pi}{4}-\frac{1}{2}\Big)\partial_y g_s - \frac{2\sqrt{2}}{3}\partial_x g_{2c},\\
&\fint_{V_u} \boldsymbol{v}\cdot\nabla_{\boldsymbol{x}} g\,\mathrm{d}\theta \approx \frac{2\sqrt{2}}{\pi}\partial_y g_1 + \Big(\frac{\pi}{4}-\frac{1}{2}\Big)\partial_x g_c + \Big(\frac{\pi}{4}+\frac{1}{2}\Big)\partial_y g_s - \frac{2\sqrt{2}}{3}\partial_y g_{2c},\\
&\fint_{V_d} \boldsymbol{v}\cdot\nabla_{\boldsymbol{x}} g\,\mathrm{d}\theta \approx -\frac{2\sqrt{2}}{\pi}\partial_y g_1 + \Big(\frac{\pi}{4}-\frac{1}{2}\Big)\partial_x g_c + \Big(\frac{\pi}{4}+\frac{1}{2}\Big)\partial_y g_s + \frac{2\sqrt{2}}{3}\partial_y g_{2c},
\end{aligned}
\tag{5.13}
$$

$$
\begin{aligned}
&\fint_{V_f} \boldsymbol{v}\cdot\nabla_{\boldsymbol{x}} h\,\mathrm{d}\theta \approx \frac{2\sqrt{2}}{\pi}\partial_x h_1 + \Big(\frac{\pi}{4}+\frac{1}{2}\Big)\partial_x h_c + \Big(\frac{\pi}{4}-\frac{1}{2}\Big)\partial_y h_s + \frac{2\sqrt{2}}{3}\partial_x h_{2c},\\
&\fint_{V_b} \boldsymbol{v}\cdot\nabla_{\boldsymbol{x}} h\,\mathrm{d}\theta \approx -\frac{2\sqrt{2}}{\pi}\partial_x h_1 + \Big(\frac{\pi}{4}+\frac{1}{2}\Big)\partial_x h_c + \Big(\frac{\pi}{4}-\frac{1}{2}\Big)\partial_y h_s - \frac{2\sqrt{2}}{3}\partial_x h_{2c},\\
&\fint_{V_u} \boldsymbol{v}\cdot\nabla_{\boldsymbol{x}} h\,\mathrm{d}\theta \approx \frac{2\sqrt{2}}{\pi}\partial_y h_1 + \Big(\frac{\pi}{4}-\frac{1}{2}\Big)\partial_x h_c + \Big(\frac{\pi}{4}+\frac{1}{2}\Big)\partial_y h_s - \frac{2\sqrt{2}}{3}\partial_y h_{2c},\\
&\fint_{V_d} \boldsymbol{v}\cdot\nabla_{\boldsymbol{x}} h\,\mathrm{d}\theta \approx -\frac{2\sqrt{2}}{\pi}\partial_y h_1 + \Big(\frac{\pi}{4}-\frac{1}{2}\Big)\partial_x h_c + \Big(\frac{\pi}{4}+\frac{1}{2}\Big)\partial_y h_s + \frac{2\sqrt{2}}{3}\partial_y h_{2c}.
\end{aligned}
\tag{5.14}
$$

Furthermore, noting (5.6), we are able to close the system (5.8), (5.10) and those equations for ρ^b, ρ^u, ρ^d and q^b, q^u, q^d using (5.12), (5.13), (5.14). If, instead of (5.11), another dependence of g, h on θ is applied, a different system can be obtained.

In summary, we get an eight-equation two-dimensional system that is similar to (3.5)–(3.8). The main assumption made here is that the methylation level is locally concentrated in each direction, but it can vary in different directions, which gives direction dependent tumbling frequency and thus chemotactic behavior. The eight-equation system we obtained can be considered as a semidiscretization in the velocity space of the original two-dimensional system (2.7). We can derive a similar PBMFT system as in (4.5)–(4.8) by asymptotics.

6. Discussion and conclusion. To seek a model at the population level that incorporates intracellular pathway dynamics, we derive a new kinetic system in this paper under the assumption that the methylation level is locally concentrated. We show via asymptotic analysis that the hydrodynamic limit of the new system recovers the original model in [27]. In particular, the quasi-static approximation on the density flux and the assumption on the methylation difference made in [27] can be understood explicitly. We show that when the average run time is much shorter than that of the population dynamics (parabolic scaling), the KS model can be achieved. Some numerical evidence is shown to present the quantitative agreement of the moment system with SPECS [22].

We remark that the idea of incorporating the underlying signaling dynamics into the classical population level chemotactic description has appeared in the pioneering works of Erban and Othmer [15, 16] and Xue and Othmer [35]. The model of the internal pathway dynamics used here is based on quantitative measurement by in vivo FRET experiments and has been proposed recently.

An open question related to the chemosensory system of bacteria still remains in the large gradient environment, in which the distribution of the methylation level is no longer locally concentrated. It would be interesting to study and improve the macroscopic model in the large gradient environment.

Acknowledgments. G.S. would like to thank Yuhai Tu for valuable discussions and Tailin Wu for his early work on simulation.

REFERENCES

[1] J. Adler, *Chemotaxis in bacteria*, Science, 153 (1966), pp. 708–716.
[2] U. Alon, M.G. Surette, N. Barkai, and S. Leibler, *Robustness in bacterial chemotaxis*, Nature, 397 (1999), pp. 168–171.
[3] W. Alt, *Biased random walk models for chemotaxis and related diffusion approximations*, J. Math. Biol., 9 (1980), pp. 147–177.
[4] H.C. Berg, *Motile behavior of bacteria*, Physics Today, 53 (2000), pp. 24–29.
[5] H.C. Berg and D.A. Brown, *Chemotaxis in Escherichia coli analysed by three-dimensional tracking*, Nature, 239 (1972), pp. 500–504.
[6] P. Biler, L. Corrias, and J. Dolbeault, *Large mass self-similar solutions of the parabolic Keller-Segel model of chemotaxis*, J. Math. Biol., 63 (2011), pp. 1–32.
[7] A. Blanchet, J.A. Carrillo, and N. Masmoudi, *Infinite time aggregation for the critical Patlak-Keller-Segel model in* $\mathbb{R}^2$, Comm. Pure Appl. Math., 61 (2008), pp. 1449–1481.
[8] A. Blanchet, J. Dolbeault, and B. Perthame, *Two-dimensional Keller-Segel model: Optimal critical mass and qualitative properties of the solutions*, Electron. J. Differential Equations, 44 (2006), pp. 1–32.
[9] N. Bournaveas and V. Calvez, *Global existence for the kinetic chemotaxis model without point wise memory effects, and including internal variables*, Kinetic and Related Models, 1 (2008), pp. 29–48.
[10] D. Bray, M.D. Levin, and K. Lipkow, *The chemotactic behavior of computer-based surrogate bacteria*, Curr. Biol., 17 (2007), pp. 12–19.
[11] A. Celani and M. Vergassola, *Bacterial strategies for chemotaxis response*, Proc. Natl. Acad. Sci. USA, 107 (2010), pp. 1391–1396.
[12] F.A.C.C. Chalub, P.A. Markowich, B. Perthame, and C. Schmeiser, *Kinetic models for chemotaxis and their drift-diffusion limits*, Monatsh. Math., 142 (2004), pp. 123–141.
[13] P. Cluzel, M. Surette, and S. Leibler, *An ultrasensitive bacterial motor revealed by monitoring signalling proteins in single cells*, Science, 287 (2000), pp. 1652–1655.
[14] R. Erban and H.J. Hwang, *Global existence results for complex hyperbolic models of bacterial chemotaxis*, Discrete Contin. Dyn. Syst. Ser. B, 6 (2006), pp. 1239–1260.
[15] R. Erban and H.G. Othmer, *From individual to collective behavior in bacterial chemotaxis*, SIAM J. Appl. Math., 65 (2004), pp. 361–391.
[16] R. Erban and H.G. Othmer, *From signal transduction to spatial pattern formation in E. coli: A paradigm for multiscale modeling in biology*, Multiscale Model. Simul., 3 (2005), pp. 362–394.
[17] F. Filbet, P. Laurencot, and B. Perthame, *Derivation of hyperbolic models for chemosensitive movement*, J. Math. Biol., 50 (2005), pp. 189–207.
[18] G.L. Hazelbauer, J.J. Falke, and J.S. Parkinson, *Bacterial chemoreceptors: High-performance signaling in networked arrays*, Trends Biochem. Sci., 33 (2008), pp. 9–19.
[19] G.L. Hazelbauer and S. Harayama, *Sensory transduction in bacterial chemotaxis*, Int. Rev. Cytol., 81 (1983), pp. 33–70.
[20] T. Hillen, *Hyperbolic models for chemosensitive movement*, Math. Models Methods Appl. Sci., 12 (2002), pp. 1007–1034.
[21] T. Hillen and H.G. Othmer, *The diffusion limit of transport equations derived from velocity-jump processes*, SIAM J. Appl. Math., 61 (2000), pp. 751–775.
[22] L. Jiang, Q. Ouyang, and Y. Tu, *Quantitative modeling of Escherichia coli chemotactic motion in environments varying in space and time*, PLoS Comput. Biol., 6 (2010), e1000735.
[23] E. Keller and L. Segel, *Model for chemotaxis*, J. Theoret. Biol., 30 (1971), pp. 225–234.
[24] J.E. Keymer, R.G. Endres, M. Skoge, Y. Meir, and N.S. Wingreen, *Chemosensing in Escherichia coli: Two regimes of two-state receptors*, Proc. Natl. Acad. Sci. USA, 103 (2006), pp. 1786–1791.

[25] B.A. Mello and Y. Tu, *Quantitative modeling of sensitivity in bacterial chemotaxis: The role of coupling among different chemoreceptor species*, Proc. Natl. Acad. Sci. USA, 100 (2003), pp. 8223–8228.
[26] T.S. Shimizu, Y. Tu, and H.C. Berg, *A modular gradient-sensing network for chemotaxis in Escherichia coli revealed by responses to time-varying stimuli*, Mol. Syst. Biol., 6 (2010), 382.
[27] G. Si, T. Wu, Q. Ouyang, and Y. Tu, *A pathway-based mean-field model for Escherichia coli chemotaxis*, Phys. Rev. Lett., 109 (2012), 048101.
[28] J.E. Simons and P.A. Milewski, *The volcano effect in bacterial chemotaxis*, Math. Comput. Model., 53 (2011), pp. 1374–1388.
[29] V. Sourjik and H.C. Berg, *Receptor sensitivity in bacterial chemotaxis*, Proc. Natl. Acad. Sci. USA, 99 (2002), pp. 123–127.
[30] A. Stevens, *Derivation of chemotaxis equations as limit dynamics of moderately interacting stochastic many-particle systems*, SIAM J. Appl. Math., 61 (2000), pp. 183–212.
[31] M.J. Tindall, P.K. Maini, S.L. Porter, and J.P. Armitage, *Overview of mathematical approaches used to model bacterial chemotaxis* II: *Bacterial populations*, Bull. Math. Biol., 70 (2008), pp. 1570–1607.
[32] M.J. Tindall, S.L. Porter, P.K. Maini, G. Gaglia, and J.P. Armitage, *Overview of mathematical approaches used to model bacterial chemotaxis* I: *The single cell*, Bull. Math. Biol., 70 (2008), pp. 1525–1569.
[33] Y. Tu, T.S. Shimizu, and H.C. Berg, *Modeling the chemotactic response of Escherichia coli to time-varying stimuli*, Proc. Natl. Acad. Sci. USA, 105 (2008), pp. 14855–14860.
[34] G. Wadhams and J. Armitage, *Making sense of it all: Bacterial chemotaxis*, Nat. Rev. Mol. Cell Biol., 5 (2004), pp. 1024–1037.
[35] C. Xue and H.G. Othmer, *Multiscale models of taxis-driven patterning in bacterial populations*, SIAM J. Appl. Math., 70 (2009), pp. 133–167.
[36] X. Zhu, G. Si, N. Deng, Q. Ouyang, T. Wu, Z. He, L. Jiang, C. Luo, and Y. Tu, *Frequency-dependent Escherichia coli chemotaxis behavior*, Phys. Rev. Lett., 108 (2012), 128101.